Int J Thermophys (2010) 31:1608–1621
DOI 10.1007/s10765-010-0810-0

Adiabatic Calorimetry Approach to Assess Thermal Influences on the Indium Melting Point

G. Failleau · N. Fleurence · R. Morice · E. Gaviot · E. Rénaot

Received: 6 March 2010 / Accepted: 4 August 2010 / Published online: 18 August 2010

Abstract Within the framework of the Euramet project 732, LCM/LNE-CNAM has recently proposed a new device to investigate the melting point of indium (156.5985 °C) by the way of an adiabatic calorimetry approach. An apparatus based on a *cell-within-cell* configuration was developed and experimentally tested. First results highlighted parasitic heat flows due to the geometrical characteristics of the cell, disturbing significantly the isothermal condition within the calorimeter. Such thermal effects were also clearly identified with a specific numerical model developed for this purpose. Considering the remarkable agreement between the model and relevant experiments, an optimization step has been carried out to design a suitable cell geometry. A new enhanced cell was subsequently fabricated and arranged within the calorimeter (indium load of 122.32 g). The purpose of this article is to introduce the thermal behavior of such a highly effective apparatus, while presenting some series of measurements; on the one hand, the melting point of indium under adiabatic conditions is studied, and on the other hand, the so-called continuous heat flow method under isothermal conditions is worked out. The obtained results are discussed and analyzed according to the impurity concentrations into the ingot (sum of individual estimate method).

Keywords Adiabatic calorimetry · Cell-within-cell · Indium · Melting

G. Failleau (✉) · N. Fleurence · R. Morice · E. Rénaot
Laboratoire Commun de Métrologie LNE-Cnam, Paris, France
e-mail: guillaume.failleau@lne.fr

G. Failleau · E. Gaviot
Laboratoire d'Acoustique de l'Université du Maine, Micro_Cap_Ouest,
UMR CNRS 6613, Le Mans, France

1 Introduction

The freezing point of indium at one standard atmosphere (156.5985 °C) is one of the fixed-points specified for use in the definition of the International Temperature Scale of 1990 (ITS-90) [1]. The maximum value of the observed temperatures following recalescence presents the advantage of being highly repeatable, typically within 0.1 mK [2–4], insofar as the freezing process is carefully driven according to suitable procedures [5]. However, investigating the uncertainty of its realization requires good knowledge of the main influencing factors, considering especially uncertainties due to thermal and chemical effects. Indeed, both factors affect simultaneously the phase transition process, and estimating their individual contributions proves to be a quite most difficult issue. Unfortunately, the liquidus point is difficult to investigate during a melting process, as the thermometer is influenced by the furnace environment. This issue could be solved by realizing adiabatic condition; then, the influence of impurities altering a given melting process could be directly observed and their effect on the liquidus point could be accurately quantified.

In this context and within the framework of the Euramet project 732, LNE is committed, since 2005, to the study of the indium fixed point with the main objective to overcome thermal influences during the fixed-point characterization. To this end, a prototype of an adiabatic calorimeter was developed at the laboratory, based on the so-called *cell-within-cell* principle [6]. The experiments pointed out the inadequate design of the first cell experimented with and other technological issues, leading to uncontrolled extraneous heat transfers. Furthermore, a specific thermal numerical model was developed and validated with experiments [7], as a most effective tool to optimize the device [8] in terms of geometry (research on the most appropriate cell structure) and thermal behavior of the whole apparatus.

The final version of the *cell-within-cell* device, significantly modified with respect to the first prototype, has been tested by realizing numerous melting processes in two different ways, namely, adiabatic and permanent heat flow methods. In order to monitor and to control the thermal conditions, a set of sensors (thermocouples and heat flow sensors) is implemented within the apparatus. Specifically, heat flow sensors were developed and implemented for this application by means of microscale devices. As shown below, such sensors have given access to real-time monitoring, providing a great deal of information during the phase transition.

After a thermal assessment of the improved *cell-within-cell* configuration, a study of the indium load thermo-chemical behavior is also proposed. Then a comparison between both thermal methods is presented.

2 Description of the Apparatus

2.1 *Cell-Within-Cell* Principle

Considering the range of medium temperatures in the ITS-90, substantial literature related to adiabatic methods had been published in the past, especially concerning the assessment of the silver freezing and melting points [9,10]. Such methods rely

on a heat pipe allowing control of the suitable homogeneity of the temperature field surrounding the fixed-point cell. The main difficulty is to adjust the furnace (or heat pipe) exactly at the same temperature as that of the fixed point during the experiment.

We propose an alternative method by the way of the *cell-within-cell* design, as the indium cell is completely surrounded by a separated external cell (the guard) that is also filled with melting indium. The whole system is arranged within an air-pulsed furnace, whose set-point temperature is adjusted just below the phase transition of the metal. In order to supply the energy required to ensure their respective phase transitions, both the guard and the cell are wrapped with specific auxiliary heaters. It is expected that when both the guard and the cell are simultaneously in a melting condition, heat exchanges between the inner cell and the guard; then, using the furnace, the heat exchange between the inner cell and guard should be almost perfectly zeroed, thus meeting the specified adiabatic condition surrounding the cell. Then the liquidus point may be determined by measuring the temperature along the solid-to-liquid transition plateau within the cell.

2.2 *Cell-Within-Cell* Configuration

2.2.1 Indium Cell

The design of the indium inner cell used in these experiments was directly tied to the results of thermal modeling [8]. Such a device has been named the "hybrid" cell. It is based on a graphite crucible (type IG210^{TM}, provided by Toyo-Tanso France®) with a 27 mm external diameter and 105 mm in height. The metal distribution within the cell is adapted to the lateral heating method used, since the load of indium (6 N purity, as recommended in [5]) is not fully surrounding the PRT well as an ingot; indeed, the bottom of the cell does not contain any metal. Then the indium is arranged in a ring around the PRT well, featuring a 3 mm thickness and a 85 mm height. The cross section of such a cell is depicted in Fig. 1.

Two thin twin auxiliary heaters (planar constantan® resistors, $(335.2 \pm 0.1)\ \Omega$, on a Kapton® substrate, $5.5 \times 3.1\ \mathrm{cm}^2$) covered with aluminum foil are arranged on the external side of the cell. Thus, heat may be supplied to the whole mass of the metal within the crucible. As an open cell configuration, beyond the metal level, the pressure of pure argon is continuously controlled at one standard atmosphere (101325 Pa) during the experiments. The mass of the indium load was measured as $m_{\mathrm{In}} = (115.98 \pm 0.02)$ g after filling.

However, before filling the cell and the upper guard, the indium shots used in the experiment have been analyzed by GDMS at CEA (Saclay, France). Table 1 summarizes the concentrations of the main impurities detected and their expected influences on the melting temperature determined by Raoult's law (Eq. 1) at the liquidus point ($F = 1$, where F is the fraction of liquid material). For each species of impurity, Table 1 lists the molar mass, the concentration in mass detected by GDMS, the mass of the considered impurity reported to the full inner cell indium load, and the associated amount of material; and finally, the molar fraction consists of the ratio of the amount of the impurity (mol) to the full indium ingot amount of material (mol).

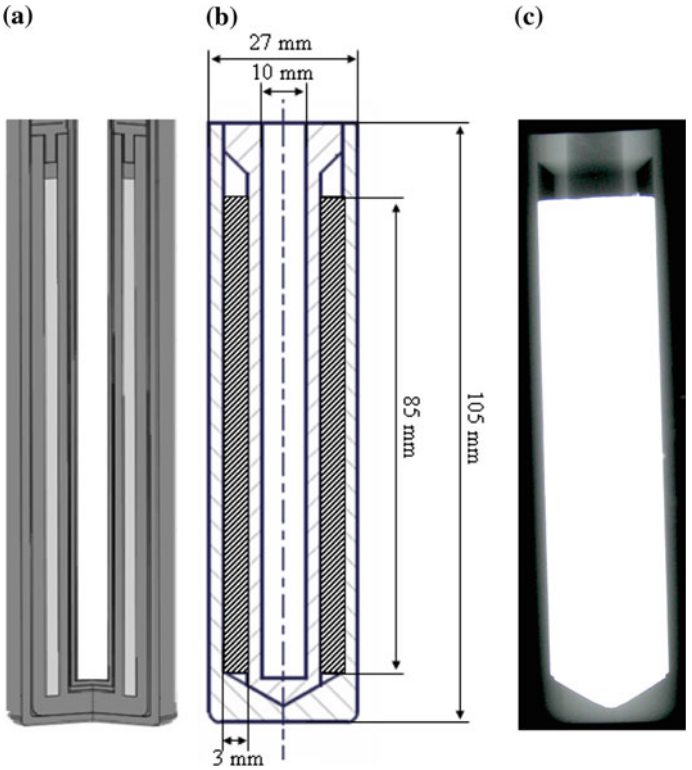

Fig. 1 Hybrid cell optimized to the *cell-within-cell* device: (a) conceptual preview assessed by thermal modeling [8], (b) technical specifications and dimensions, and (c) indium ingot view under X-ray after filling

Table 1 Summary of the main impurities detected in the indium by GDMS; cryoscopic temperature decrease or increase expected for each impurity at the liquidus point

	k	M ($g \cdot mol^{-1}$)	C ($\mu g \cdot g^{-1}$)	m (g)	n (mol)	Molar fraction	ΔT (K)
In-Fe	0.0599	55.85	85	9.86×10^{-6}	1.77×10^{-7}	1.75×10^{-7}	-7.67×10^{-5}
In-Al	0.2703	26.98	35	4.06×10^{-6}	1.50×10^{-7}	1.49×10^{-7}	-5.07×10^{-5}
In-Cd	1.3705	112.40	3	3.48×10^{-7}	3.10×10^{-9}	3.06×10^{-9}	5.30×10^{-7}
In-Cu	0.0561	63.54	45	5.22×10^{-6}	8.22×10^{-8}	8.13×10^{-8}	-3.58×10^{-5}
In-Ga	0.6318	69.70	5	5.80×10^{-7}	8.32×10^{-9}	8.24×10^{-9}	-1.42×10^{-6}
In-Ni	0.0285	58.71	35	4.06×10^{-6}	6.92×10^{-8}	6.85×10^{-8}	-3.10×10^{-5}
In-Pb	0.3973	207.19	60	6.96×10^{-6}	3.36×10^{-8}	3.33×10^{-8}	-9.35×10^{-6}
In-Sn	0.7906	118.69	110	1.28×10^{-5}	1.08×10^{-7}	1.06×10^{-7}	-1.04×10^{-5}
In-Ti	0.1633	47.90	1.5	1.74×10^{-7}	3.63×10^{-9}	3.60×10^{-9}	-1.40×10^{-6}
In-Zn	0.6507	65.37	30	3.48×10^{-6}	5.32×10^{-8}	5.27×10^{-8}	-8.59×10^{-6}
In	–	114.82	106	115.98	1.01	Overall ΔT	-2.25×10^{-4}

$$\Delta T = \frac{-\left(1 - k_{\text{imp}}\right)}{A} C_{\text{imp}}, \tag{1}$$

where A is the first cryoscopic constant and k_{imp} and C_{imp} are, respectively, the equilibrium coefficient and the molar fraction of the considered impurity.

All equilibrium coefficients have been calculated by means of MTDATA software [11] available as a probing version. The first cryoscopic constant chosen for the indium is $A = 0.002143\,\text{K}^{-1}$, as recommended by the *Comité Consultatif de Thermométrie* [12].

2.2.2 Surrounding Environment

Practically, the configuration is shaped as two graphite guard cells enclosed in one another and filled with indium (Fig. 2). Indeed the fixed-point cell is inserted within an indium guard (so-called 'main lateral guard,' diameter of 66 mm and height of 238 mm). Moreover, a second indium guard (so-called 'upper guard,' diameter of 27 mm and height of 105 mm) is arranged above the indium cell. Both the cell and upper guard take place in a quartz sheath closed by a tight flange; this system allows operation under vacuum (5×10^{-4} mbar) as a cleaning procedure, prior to maintaining a constant pressure of argon (1 atm). The upper guard is designed like the cell, but with an indium height of 90 mm and a load of metal weighed after filling ((122.32 ± 0.02) g). The whole assembly is depicted in Fig. 2.

In the central well, the PRT is not directly in contact with the graphite material. An inner quartz pipe frosted over its whole height (to prevent the light-piping effect) closes the quartz bulb system on the inside.

The upper guard is wrapped with two auxiliary heaters (resistive wire double coils sheathed by an aluminum foil, with a cross section of 1 mm and a linear resistance of $20\,\Omega \cdot \text{m}^{-1}$). On the upper guard top zone, the heater overlaps the

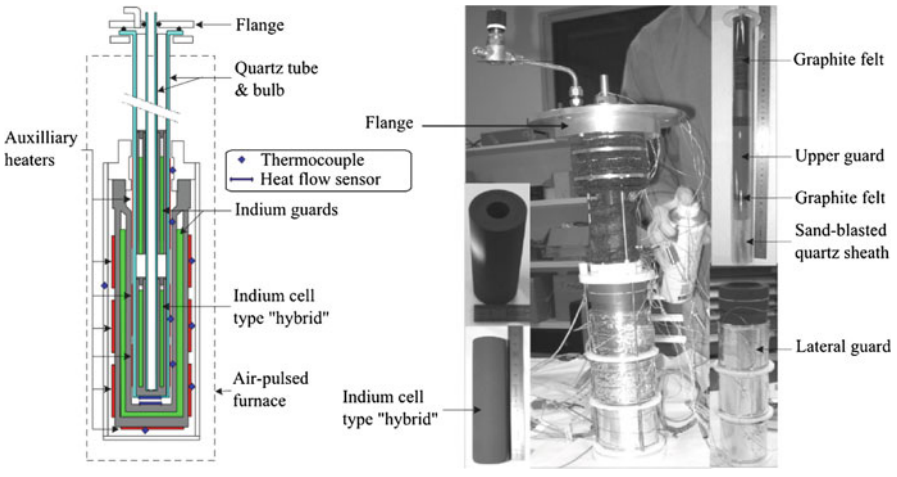

Fig. 2 *Cell-within-cell* device, principle, and overview of the whole device

upper guard height by 3 cm with an electric resistance measured after assembly of $(126.7 \pm 0.1)\ \Omega$. Furthermore, on the lower zone, the second (and main) heater covers 7 cm of height, the electrical resistance was also measured after assembly $((334.1 \pm 0.1)\ \Omega)$.

The main lateral guard that contains 1.1 kg of indium surrounds the whole inner system enclosed by the quartz bulb. Four auxiliary heaters (resistive wire double coils sheathed by an aluminum foil, cross section of 1 mm, and linear resistance of $20\ \Omega \cdot \mathrm{m}^{-1}$) are arranged around this guard. They act as three active heating zones on the lateral side, and a fourth at the bottom. This device, designed to be used at atmospheric conditions, is enclosed in a stainless-steel outer casing. The whole assembly is placed in an air flow furnace whose temperature is controlled within 0.5 °C below the melting point. Only one control loop is used to set the furnace temperature. For the *cell-within-cell* apparatus, the operator manually controls each heater. Nevertheless, the driving interface used with the calorimeter has a semi-automatic function to control. The operator can program a time loop (repeating to infinity or for a specified number of times) to provide, for each of the auxiliary heaters, sequences of continuous or pulsed heating following the experimental protocol chosen.

2.3 Sensors and Measurement Devices

2.4 Temperature Monitoring

A specific movable type K thermocouple is pressed against the external side of the stainless-steel outer casing in order to control the furnace temperature gradients.

The fixed-point temperature measurements are performed with a calibrated type R800-2 Chino standard platinum resistance thermometer. The probe sensitivity is inferred from the calibration $((0.097 \pm 0.004)\ \Omega \cdot \mathrm{K}^{-1})$ and the electrical resistance value of the SPRT at the triple point of water is measured $((25.39498 \pm 0.00002)\ \Omega)$. The SPRT is interfaced with a high-quality ASL F900 bridge. An external standard resistance $((49.99683 \pm 5 \times 10^{-5})\ \Omega)$, connected to the bridge, is placed in an isothermal enclosure controlled at 23 °C with a 100 Ω platinum thermometer.

The SPRT is periodically checked at the melting point of gallium during the experiments. Then, the obtained results are systematically referenced to the gallium point.

2.4.1 Heat Flow Sensors

Prior to design of the hybrid configuration, the first tests with the original prototype had pinpointed a problem of maintaining the adiabatic condition at the bottom of the device [6]. Such a shortcoming was due to the large mass of indium at the bottom on the guard that remained permanently frozen. Conversely, no such problem was observed on the lateral part of the guard. Thus, to allow permanent monitoring on the bottom critical area, two heat-flow sensors (HFSs) have been implemented. As self-generating sensors, HFSs rely on thin planar thermopiles, covered with two coppered Kapton® foils with a total thickness averaging 0.5 mm. The main sensor is directly pressed against the bottom of the quartz bulb, as the second one is

simply arranged on the bottom of the main guard (cf. Fig. 2). Such specific devices, commercialized for versatile industrial purposes and generally limited under 250 °C, supply low-noise signals ($Z = 80\,\Omega$) that can be monitored with a simple electronic low-drift chopper-stabilized amplifier (TLC 2652, Gain = 50, offset measured and compensated by software), according to their significant sensitivity averaging $7.2\,\mu V \cdot W^{-1} \cdot m^2$.

3 Measurements

3.1 Validation of the Adiabatic Conditions

A first and major step in our experiments was to assess and validate the adiabatic condition within the *cell-within-cell* device. In the following paragraphs, each experimental procedure begins systematically with starting the melting of the indium within the guards. The air-pulsed furnace temperature is adjusted to a point 0.5 °C below the indium melting point. Then, a first heat pulse is supplied by the heater placed on the top zone of the main lateral guard. As the thermocouple signal shows the generation of a solid-to-liquid interface, supplementary heat pulses are supplied by the other available heaters. Then, the indium in the upper guard is also ensured to be in its phase transition by means of its associated heaters. Finally, the cell achieves an isothermal condition upon all its boundaries.

A single heat pulse is necessary to drive the indium cell at the melting plateau (0.61 W for 750 s). When the heaters are switched-off, and after reaching thermal equilibrium as checked by the SPRT in the cell well, the signal from the main HFS may be considered. Figure 3 shows a typical initialization of such a melting plateau by applying this procedure. In fact, a set of two heat pulses must be applied to the cell to achieve the ideal adiabatic condition in terms of heat flow detection. Since the amplitude of the HFS signal is directly proportional to the heat flow magnitude detected, it is well established that an observed zeroed emf is strong evidence of the physical absence of heat exchange [13]. The signal depicted in Fig. 3 illustrates such a case. This observation stands as a first significant step to assess the adiabatic condition in the *cell-within-cell* calorimeter, as the cell and its guards are both in their respective phase transitions.

A second series of measurements allowed to investigate the achievement of the adiabatic condition; then, the temperature profile was measured along the well height within the cell during the melting process. The results are shown in Fig. 4. As a matter of practice, two measurements had been performed at the limits of the plateau (near the solidus point at $F < 0.20$, and near the liquidus point at $F > 0.85$). A series of measurements had been carried out for several values of F, with $0.20 < F < 0.85$. Such measurements being extremely repeatable, only one example of them is illustrated in Fig. 4.

When the plateau observed in the cell is clearly in progress, the temperature profile is in full agreement with the hydrostatic pressure effect. The obtained pattern demonstrates the absence of extraneous thermal effects during this part of the melting process, according to the adiabatic condition highlighted by the HFS.

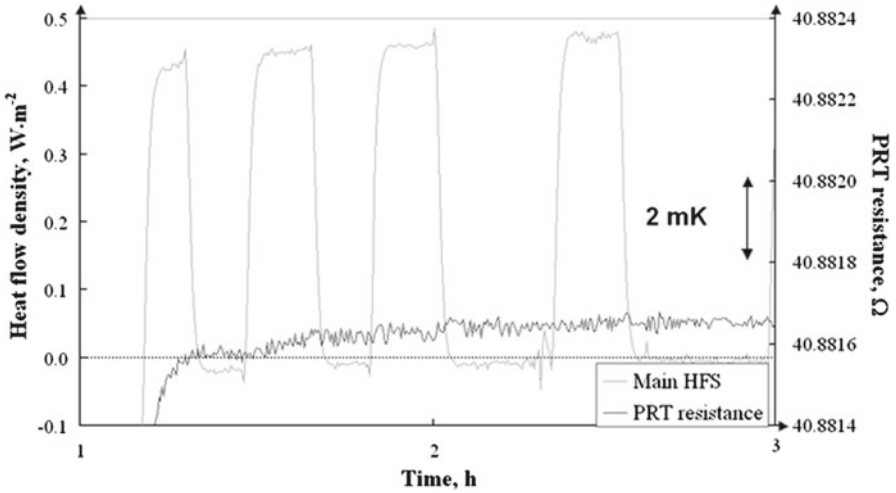

Fig. 3 Zeroed heat-flow density measured by the main HFS at the beginning of the plateau

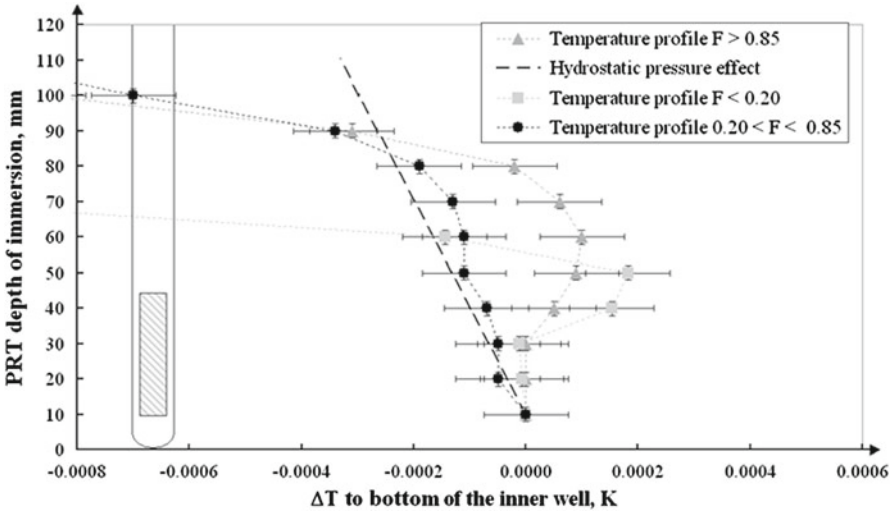

Fig. 4 Temperature profiles along the cell inner well during a melting plateau for several values of F

Close to both ending and starting points of the plateau, the temperature profile is altered, because of probable discontinuities along the solid-to-liquid interface for the extreme values of F. Thus, any remaining heat flow due to the thermal relaxation of the heater, after supplying energy, is enough to disturb the profile at the beginning of the plateau. The overheated metal in its liquid phase may be assumed to cause the disturbances observed in the temperature profile near the end of the plateau.

3.2 Realizing the Melting Point of Indium

3.2.1 Permanent Heat Flow-Operating Mode

After onset of the phase transition on the whole guard system, a continuous heat flow was supplied to the inner cell with its auxiliary heaters (0.21 W). Figure 5a shows a typical melting plateau obtained under the permanent heat flow operating mode. The heat flow sensor signal allows to detect with great accuracy the beginning (solidus point) and the end (liquidus point, or the melt-off) of the complete melting process,

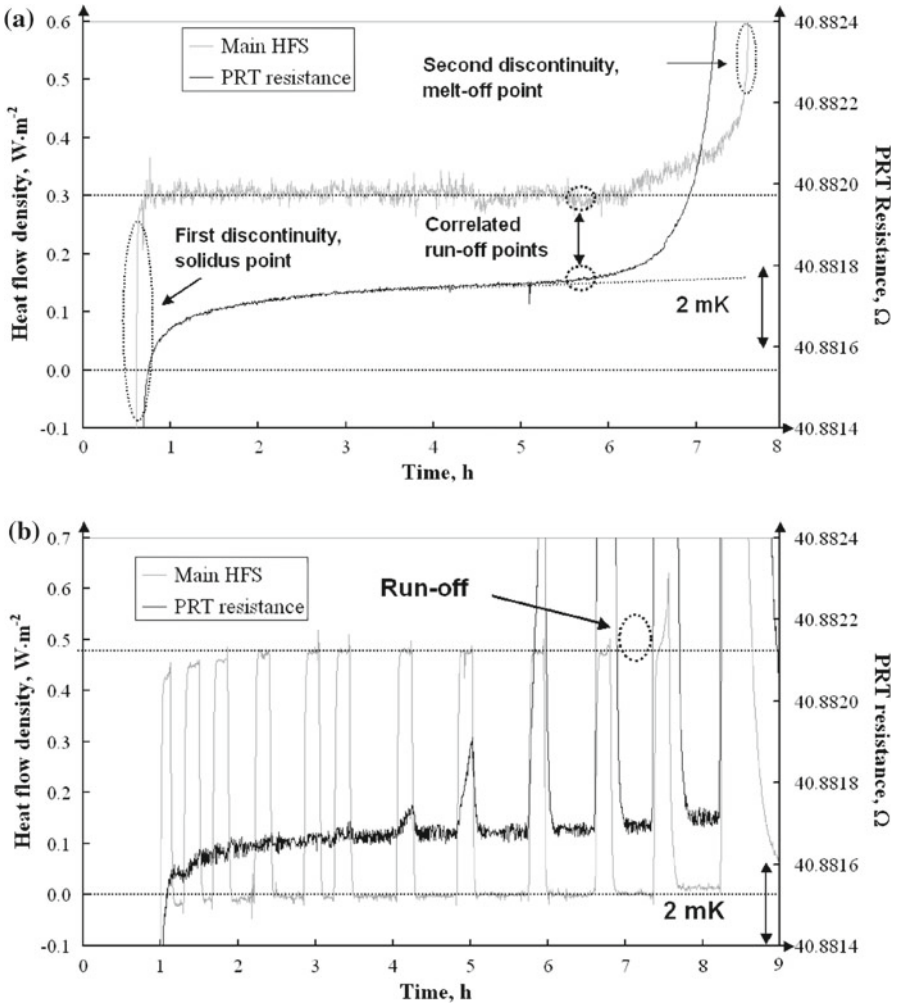

Fig. 5 (a) Typical melting plateau, represented in heat-flow density and temperature, obtained by the permanent heat flow operating mode and (b) melting plateau observed with the adiabatic operating mode, and represented with the associated heat-flow density measurement

by the presence of two discontinuities. Since the inner cell heaters are continuously switched-on, the measured heat flow is different from zero. Obviously, we have to stress what would happen if the auxiliary heater was switched-off along the plateau; in other words, the adiabatic condition (with a zeroed heat flow) must be verified. Specific measurements have highlighted a residual part of the heat flow supplied by the heaters getting through the inner cell bottom to the SPRT. Along the whole melting plateau, a constant shift-up of the SPRT resistance measured value was observed, corresponding to a 0.2 mK equivalent temperature. We will call this phenomenon the "residual heat effect" (RHE). In fact, a part of the heat supplied by the heaters is transmitted by conduction through the quartz sheath and by crossing the graphite at the bottom of the inner cell, uncovered by the metal. The constant level of the heat flow observed during the melting process is relevant with a thermal self-stabilization of the system when the solid-to-liquid interface is maintained. Near the end of the plateau, about 2 h before the second discontinuity observed by way of the HFS, the heat-flow density level is marked with a continuous drift with a constant slope averaging $1\,\mathrm{W}\cdot\mathrm{m}^{-2}\cdot\mathrm{h}^{-1}$ (cf. Fig. 5a). This phenomenon starts at a specific point, correlated with an observation commonly made with temperature measurements, with the so-called run-off point. Compared with the steady-state prior to the run-off point, such a continuous drift of the heat-flow density level results in an altered thermal regime within the inner cell, at the end of the plateau. It is clear that an increasing part of the energy supplied by the heater is leaked into the guard at the end of the melting process, as the efficient fraction of the energy incoming in the metal (as a latent heat exchange) is simultaneously decreased [14]. Such a simple consideration clearly shows that the heat transfer rate between the metal and its environment (auxiliary heaters in our case) cannot be considered as an invariant quantity during a melting plateau; thus, in any classical analysis, a significant error is systematically developed with regard to the computation of the F values along the whole transition process.

3.2.2 Adiabatic Operating Mode

The second operating mode relies on the supply of discrete amounts of heat introduced within the inner cell as the whole guard system is maintained at its phase transition. Each heat pulse is followed with a return to thermal equilibrium of the system. When the temperature is completely stabilized, a relevant measurement could be considered with the SPRT. In this way, the values are obtained under an adiabatic condition, as the inner cell and its surrounding guards have reached the same constant temperature. A melting plateau is typically performed for a duration averaging 10 h. Then, 11 heat pulses (total supplied power of 0.61 W for 750 s) are needed to cross the full phase transition of the indium.

As illustrated in Fig. 5b, the heat-flow density is measured simultaneously with the temperature, by means of the main HFS. The first heat pulse allows initiation of the melting plateau. Then, the HFS signal gives relevant information about the progress of the melting process. First of all, the level of the heat flow density between two heat pulses when the system reaches thermal equilibrium is equal to zero, proving a real adiabatic condition (no heat exchanged) at the inner cell boundaries. Secondly, despite the fact that the heat pulses rigorously supply the same amount of energy to

the cell, the heat flow density level observed when the heaters are switched-on vary at the early beginning of the plateau until the third heat pulse is applied. This results in a transient thermal regime, with discontinuities marking the solid-to-liquid interface and associated chemical and mechanical rearrangements. In the same way, it was observed in the permanent heat flow operating mode, that the energy supplied by the heaters to the metal as the amount of the energy effectively converted into latent heat is not an invariant quantity during the whole melting process. In fact, the conventional computation of the F value, as the ratio of the heat supplied by the heaters to the whole melting enthalpy of the ingot, is marked with a significant error. In fact, F values prove to be over-estimated at the beginning of the plateau.

3.2.3 Influence of the Freezing Mode

As a matter of practice, the impurity distribution into the ingot and the freezing velocity are expected to alter the melting plateau pattern. We propose an experimental approach to investigate such effects, by carrying out an adequate series of cross experiences with the *cell-within-cell* device. The cell is systematically brought and maintained to a full liquid state for more than 24 h, to optimize the impurity diffusion within the liquid phase, or is directly frozen.

To study the influence of the freezing mode, two different procedures are exploited. Fast freezing (<10 min) is obtained by supplying a gas jet (argon, $1\,\mathrm{L}\cdot\mathrm{min}^{-1}$) in the cell inner well. The guards are in a solid state, and the furnace is set at a point 3 K below the phase transition. Conversely, to proceed with slow freezing (above 10 h), the furnace is kept 3 K below the phase transition and the guards are operated when the maximum of overcooling is observed in the cell. At the same time, the furnace temperature set point is adjusted to a point 0.5 K below the phase transition. Details about the cross experiences, also described in [15], are summarized in Table 2.

3.3 Main Results

The melting plateaus obtained with both different freezing modes are shown in Fig. 6. Each one is bounded between the solidus and liquidus points, detected with an HFS. Thus, it is possible to plot the melting curve as a function of F. To allow an easy comparison between the curves, the points $T(F = 50)$ are arbitrarily chosen, regarding their quite relevant repeatability, as reference points [15]. The excellent unexpected matching observed between the whole set of curves demonstrates the influence of the freezing mode, but does not seem to alter the melting process. Moreover, the indium

Table 2 Summary of the cross experiences realized to detect a prospective influence of the freezing mode applied before indium cell melting

	Fast freeze (<10 min)	Slow freeze (above 10 h)
Cell frozen directly after complete melting	Series 3	Series 5
Cell kept more than 24 h in liquid state before freezing	Series 4	Series 1,2

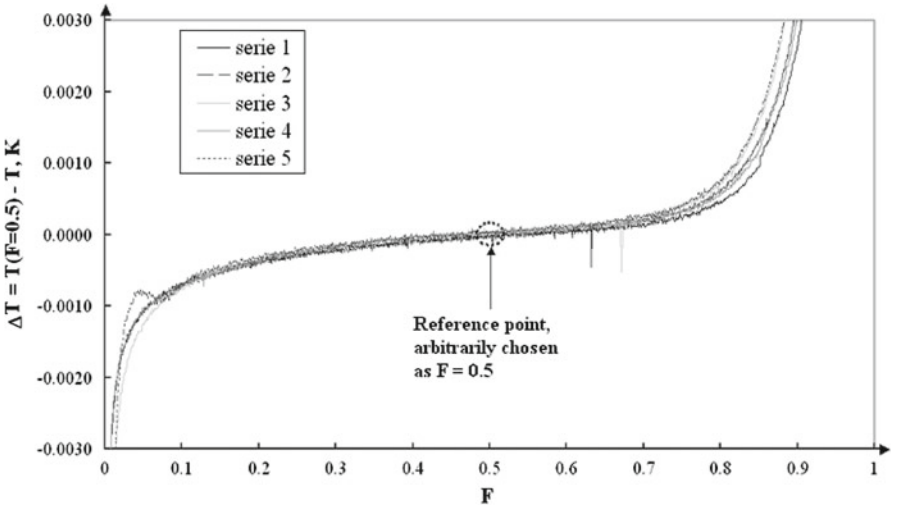

Fig. 6 Combined influences of segregation modes and diffusion duration in liquid phase on the indium melting curves

cell is immune to the initial condition of the setup, that is to say, the prospective diffusion in the liquid phase for kinetic freezing before melting.

Numerous series of measurements have been realized by using both the permanent heat flow and adiabatic operating modes. From the equilibrium coefficients detailed in Table 1, the cryoscopic temperature decrease expected by Raoult's law has been computed considering the following *sum of individual estimate* (SIE) method [16]:

$$\Delta T = \sum_{\text{imp}} -\frac{(1 - K_{\text{imp}})}{A} C_{\text{imp}} F^{-(1-K_{\text{imp}})}, \tag{2}$$

where ΔT is the difference between the measured temperature $T(F)$ and the melting temperature of the ideal pure indium, extrapolated from the $1/F$ plots at $1/F = 0$ considering the domain $1.2 < 1/F < 5$, as recommended in [17].

As shown in Fig. 7, a few $1/F$ plots obtained with both operating modes are compared with the theoretical law. The plots, corresponding to permanent heat flow, are systematically corrected with regard to the RHE previously defined. The perfect matching between experimental points and theory may be clearly highlighted. Then, the equilibrium coefficients presented in Table 1 seem to be quite relevant to our knowledge.

As a simple observation, the plots obtained under the permanent heat flow operating mode are depicting an altered thermal regime that appears far from the end of the plateau ($1/F = 1.5$ for 65 % of formed liquid). In comparison, the plots obtained under the adiabatic condition are better matching the theoretical law until $1/F = 1.1$ ($F = 90\,\%$). The error affecting the liquidus point temperature determination should decrease significantly by using the adiabatic operating mode.

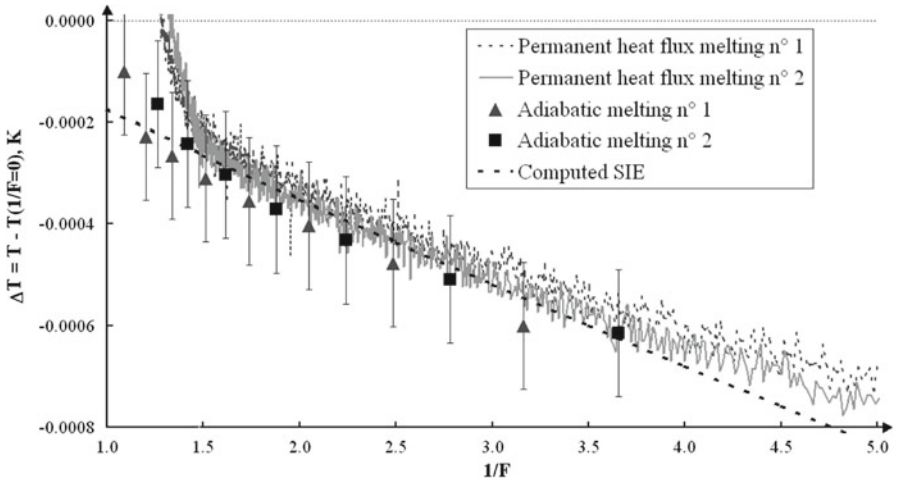

Fig. 7 $1/F$ plots, comparison of several melting processes obtained under the two operating modes, and the computed SIE

4 Conclusion and Perspective

The improved *cell-within-cell* device designed for characterization of the indium melting point has demonstrated a real efficiency to establish very rigorously the adiabatic condition.

The two operating modes (adiabatic and permanent heat flow) previously described have shown great repeatability with regard to the measurement, and their treatments in terms of $1/F$ plots have confirmed excellent agreement with the SIE method of correction. Thus, as thermal effects can be controlled in a stringent way by the *cell-within-cell* measurement approach, the chemical phenomena can be rigorously studied and accurately quantified.

As a matter of experience, with the indium cell, no influence of either the freezing mode or the time spent in the liquid phase after complete melting has been observed. It seems that the indium melting point is unaffected by the ingot freezing history. Another study, recently published [18], has testified to the origin of the limited indium sensitivity to impurity effects.

The implementation of heat flow sensors at strategic and critical positions in the calorimeter have demonstrated their importance in thermal monitoring of the apparatus. So, beyond monitoring, they have been shown to provide accurate detection of both the physical starting and ending points of the phase transition. Currently, with the great deal of data recorded during these experiments, a new method of analysis of the transition and associated conceptual developments is under investigation. The prospective, now expected soon, should give a new approach and additional understanding of phase transitions at temperature fixed points, especially in terms of thermodynamic considerations and kinetic distribution of the energy during melting or freezing processes.

Acknowledgments The authors wish to express their very grateful acknowledgments to A. Lesauvage and J. C. Barbaras (LNE-DRTI), senior engineers, for their valuable contributions and their timely advice concerning mechanics and thermals, and for the technical development of the final *cell-within-cell* device. G. Ledortz (LNE-DRTI), senior engineer, is also acknowledged for his development of the remarkable monitoring and drive software used during these experiments.

References

1. H. Preston-Thomas, Metrologia **27**, 3 (1990)
2. B.W. Mangum, Metrologia **26**, 211 (1989)
3. C. Rauta, E. Renaot, M.H. Valin, M. Elgourdou, F. Adunka, A. van der Linden, A. Steiner, J. Bartu, M. Smid, M. Sindelar, E. Tegeler, U. Noatsch, J-U. Holtoug, V. Chimenti, M. Anagnostou, T. Weckstrøm, G. Sutton, R. Rusby, F. Pavese, P.P.M. Steur, P. Marcarino, M.J. de Groot, E. Filipe, I. Lobo, J. Ivarsson, S. Duris, J. Bojkovski, M. Hiti, S. Ugur, A.K. Dogan, E. Grudniewicz, Metrologia **45** (Tech. Suppl. 03001) (2008). doi:088/0026-1394/45/1A/03001
4. B.N. Oleinik, A.G. Ivanova, M.M. Dvinianinov, V.A. Zamkovets, in *Rapport du Comité Consultatif de Thermométrie*, Doc. CCT/84-1, BIPM (1984)
5. BIPM, Supplementary Information for the ITS-90 (Pavillon de Breteuil, Sèvres, 1990)
6. R. Morice, G. Bonnier, J.C. Barbaras, N. Fleurence, V. Le Sant, P. Ridoux, J.R. Filtz, Int. J. Thermophys. **29**, 1785 (2008)
7. V. Le Sant, R. Morice, G. Failleau, Int. J. Thermophys. **29**, 1772 (2008)
8. G. Failleau, V. Le Sant, R. Morice, P. Ridoux, in *Proceedings of Tempbeijing 2008*, Acta Metrologica Sinica **29** (2008)
9. G. Bonnier, E. Reanot, Metrologia **33**, 363 (1996)
10. J. Ancsin, Metrologia **38**, 1 (2001)
11. R.H. Davies, A.T. Dinsdale, J.A. Gisby, J.A.J. Robinson, S.M. Martin, in *MTDATA - Thermodynamic and Phase Equilibrium Software* from the National Physical Laboratory, CALPHAD **26**, 27 (2002)
12. S. Rutdsch, in *Rapport du Comité Consultatif de Thermométrie*, Doc. CCT/05-04/rev, BIPM (2005)
13. C.J. Shirtliffe, R.P. Tye, in *ASTM Special Tech. Pub.* 879 (ASTM, Philadelphia, 1985)
14. E. Gaviot, G. Failleau, R. Morice, L. Camberlein, F. Polet, B. Bêche, Metrologia **47**, 349 (2010)
15. G. Failleau, in *Etude et Développement d'un Calorimètre Adiabatique Pour la Caractérisation du Point-Fixe de L'indium. Application des Mesures Fluxmétriques a L'Optimisation des Cellules Calorimétriques*, Thèse de Doctorat (L'Université du Maine, Le Mans, France, 2010)
16. D. Ripple, A. Pokhodun, P. Steur, G. Strouse, O. Tamura, in *Rapport du Comité Consultatif de Thermométrie*, Doc. CCT/05-08, BIPM (2005)
17. G.F. Strouse, in *Rapport du Comité Consultatif de Thermométrie*, Doc. CCT/03-19, BIPM (2003)
18. M. Fahr, S. Rutdsch, Metrologia **46**, 423 (2009)